

Resonant impurity states in chemically disordered half-Heusler Dirac semimetals

J. Kiss, S. W. D'Souza, L. Wollmann, C. Felser, and S. Chadov

Max-Planck-Institut für Chemische Physik fester Stoffe, Nöthnitzer Str. 40, 01187 Dresden, Germany

K. Chadova, D. Ködderitzsch, J. Minár, and H. Ebert

Dept. Chemie, Ludwig-Maximilians-Universität, Butenandtstr. 11, 81377 München, Germany

We address the electron transport characteristics in bulk half-Heusler alloys with their compositions tuned to the borderline between topologically nontrivial semi-metallic and trivial semiconducting phases. The precise first-principles calculations based on the coherent potential approximation (CPA) reveal that all the studied systems exhibit sets of dispersionless impurity-like resonant levels, with one of them being located right at the Dirac point. By means of the Kubo formalism we reveal that the residual conductivity of these alloys is strongly suppressed by impurity scattering, whereas the spin Hall conductivity exhibits a large value which is comparable to that of Pt, thereby leading to divergent spin Hall angles.

Keywords: CPA, topological insulator, resonant impurity, Kubo formalism, spin current

I. INTRODUCTION

The subgroup of the half-Heusler materials with a ternary composition (consisting of an alkali- or an early transition element, main-group element and a late transition element) contains a large family of nonmagnetic semiconductors and nonmagnetic semimetals. Exceptions are the half-Heuslers containing Mn as an early transition element (which always tends to develop a strong localized magnetic moment), or those, whose number of valence electrons differs from 18 per formula unit. The variety of possible ternary atomic combinations makes the half-Heusler family large enough to include topologically distinct classes of materials - trivial (typically light compounds exhibiting a direct band gap at the Γ point of the Brillouin zone) and nontrivial systems (semimetals or gapless semiconductors exhibiting the band inversion at the Γ point) with respect to the \mathbb{Z}_2 invariant, which have been studied in details in Refs. [1–3]. On the other hand, those systems which might lie at the borderline between the nontrivial and trivial systems, cannot be strictly identified, despite that they may exist within this group. The reason for this is quite clear: in contrast to e.g., Weyl semimetals, for the half-Heusler and the related zinc-blende structure types there are no strict symmetry arguments which would guarantee the stability of the topological transition state. Because of that, the emergence of linear-dispersive states which might manifest the topological phase transition in the half-Heusler systems can be expected only at the nontrivial/trivial interfaces. Nevertheless, the borderline bulk systems in principle can be constructed within the Heusler class, since there exist several physically reasonable “adiabatic paths” which continuously link both topological classes, such as pressure and chemical substitution. Some of such systems, as e.g., the zinc-blende $\text{Hg}_{0.83}\text{Cd}_{0.17}\text{Te}$, where already quite clearly identified in the past [4, 5] and also studied recently [6]. Their Dirac cones centered at the Γ point of the Brillouin zone repre-

sent a separate class of massless fermions (Kane fermions) which cannot be reduced to any well-known case of massless particles in quantum electrodynamics [6]. In addition, since the Heusler-based topological systems attract growing interest due to the sensitivity of their properties and simultaneous stability of the structure with respect to the chemical content, we will model the chemical variety using first-principles calculations by bringing the system into the topological borderline regime to study its residual transport characteristics.

II. MODELING

After first theoretical attempts to classify the half-Heusler semiconductors in the sense of the topological \mathbb{Z}_2 invariant [1, 2], many similar calculations have been performed. Since the numerical methods as well as the ways in which they have been applied are very different, the results for a particular half-Heusler composition may vary a lot. On the other hand, all these results exhibit the same general trend: the light half-Heuslers appear to be trivial, whereas the heavy ones are most probably nontrivial. In this context, there is no guiding principle used to select particular systems we are going to link by an appropriate chemical substitution, but we based our modeling using the systems which are already known. The first system is the heavy half-Heusler LaPtBi [7], which in most of the calculations exhibits a band-inversion [8] indicating that it represents a typical nontrivial semimetal. The lighter half-Heusler LaPdBi [9], which in calculations exhibits a small indirect band gap [1–3], will serve as a representative trivial system. Since both compounds have the same crystal structure, it might be possible to generate a series of isostructural $\text{La}(\text{Pt}_{1-x}\text{Pd}_x)\text{Bi}$ alloys, by continuously varying x from 0 to 1. Such series will necessarily contain a specific composition corresponding to the topological transition. Theoretically we can efficiently search for it by performing a series of calculations for different con-

centrations and inspecting the change of the electronic structure. Similar calculations were performed already for the binary systems, as e.g. for the similar class of the zinc-blende [10] and the rock-salt semiconductors [11, 12].

III. CALCULATIONS

We performed our calculations using the relativistic Green function SPR-KKR method [13] in combination with the CPA alloy theory [14, 15] to study the non-stoichiometric compositions, and applying the spherical approximation (ASA) for the atomic potentials. The exchange-correlation functional was treated within the generalized gradient approximation (GGA) [16]. The lattice constant as a function of x was interpolated linearly between the experimental values for the concentrations $x = 0$ and 1. Since the disorder breaks translational symmetry, the electronic eigenstates are not localized in the momentum space. In this case, in order to visualize the electronic structure we will use the concept of the Bloch spectral function (BSF), which provides a distribution of the electron spectral weight within energy-momentum space, being defined as a Fourier transform of the real-space Green function $G(\vec{r}, \vec{r}', E)$:

$$A(\vec{k}, E) = -\frac{1}{\pi N} \text{Im} \sum_{n,m=1}^N e^{i\vec{k}(\vec{R}_n - \vec{R}_m)} \times \int d^3r \langle G(\vec{r} + \vec{R}_n, \vec{r} + \vec{R}_m, E) \rangle,$$

where $\langle \rangle$ denotes the CPA average and $\vec{R}_{n(m)}$ are the atomic lattice vectors. $A(\vec{k}, E)$ can be interpreted as a \vec{k} -resolved DOS (density of states) function, since

$$n(E) = \frac{1}{\Omega_{\text{BZ}}} \int_{\Omega_{\text{BZ}}} d^3k A(\vec{k}, E),$$

with $n(E)$ being the total DOS, and Ω_{BZ} the Brillouin zone volume. For the compound with ideal translational symmetry, the Green function contains poles on the energy axis, which results into a set of the δ -function peaks for the DOS, BSF, or other energy-dependent quantities. To keep them for pure systems as continuous energy functions, they are calculated via the Green function which is slightly misplaced from its poles by adding a small imaginary offset $\text{Im}E = \delta$ to the energy argument. If disorder treated by the CPA, the effective Green function does not contain poles on the real energy axis due to the effective self-energy, which strictly speaking contains a non-zero imaginary part at any energy value by making the effective Green function to be analytical everywhere on the real energy axis. Nevertheless, since here we are dealing with semimetals, their spectral weight close to the Fermi energy is very small, which leads to a severe reduction of the imaginary part of the corresponding self-energy. To avoid numerical instabilities which might be possible

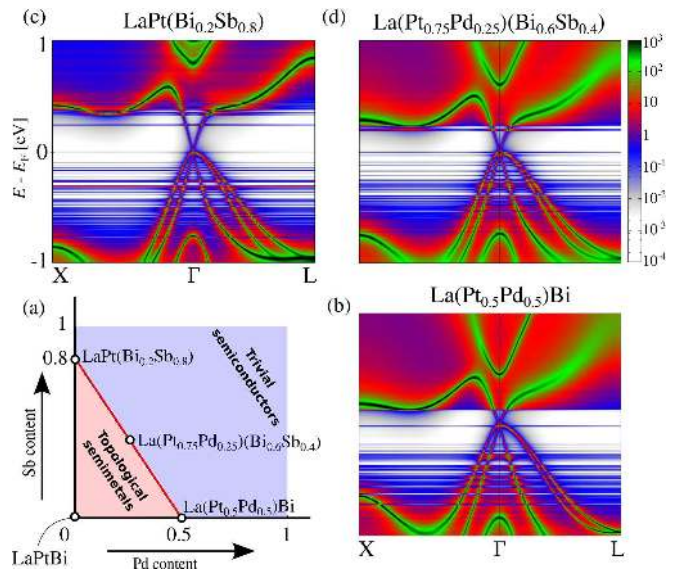


FIG. 1: (a) Compositional tuning. By taking LaPtBi as a starting point, we generate the series of $\text{La}(\text{Pt}_{1-x}\text{Pd}_x)\text{Bi}$ alloys, in which the topological phase transition occurs at $x \approx 0.5$. Analogously, within $\text{LaPt}(\text{Bi}_{1-y}\text{Sb}_y)$ series, the transition occurs at $y \approx 0.8$. These two compositions generate a continuous set of borderline materials $\text{La}(\text{Pt}_{1-x}\text{Pd}_x)(\text{Bi}_{1-y}\text{Sb}_y)$: $y \approx 0.8 - 1.6 \cdot x$, whose compositions are placed along the red line separating the nontrivial and trivial systems (light-red and light-blue colored areas, respectively). (b), (c) and (d) represent the BSFs, calculated for three borderline compositions: $\text{La}(\text{Pt}_{0.5}\text{Pd}_{0.5})\text{Bi}$, $\text{LaPt}(\text{Bi}_{0.2}\text{Sb}_{0.8})$ and $\text{La}(\text{Pt}_{0.75}\text{Pd}_{0.25})(\text{Bi}_{0.6}\text{Sb}_{0.4})$, respectively. The spectral intensity distribution corresponds to the logarithmic color scale, shown at the right side of (d).

in such a regime for the BSF calculation we add to the energy a very small imaginary offset $\delta = 0.01$ meV.

IV. ELECTRONIC STRUCTURE

Schematically the search for the borderline compositions is shown in Fig. 1a. We start with LaPtBi which belongs to the nontrivial phase (point at the origin) and continuously substitute Pt by Pd going towards LaPdBi ($x = 1$). The transition into the trivial phase occurs at about $x = 0.5$, i.e. for $\text{La}(\text{Pt}_{0.5}\text{Pd}_{0.5})\text{Bi}$. The corresponding BSF is depicted in Fig. 1b. Just to demonstrate the flexibility and variability of the ternary half-Heusler systems, we can select another chemical link from LaPdBi into the trivial phase, by substituting the main-group element. For instance, we can continuously substitute Bi by Sb generating another set of Heusler series, $\text{LaPt}(\text{Bi}_{1-y}\text{Sb}_y)$, which crosses the topological transition point at about $y = 0.8$; the corresponding BSF is depicted in Fig. 1c. We notice, that the stoichiometric compound LaPdSb ($y = 1$) exists in reality as well, however it crystallizes in the hexagonal structure [17]. To establish the correspond-

ing series, we used the cubic half-Heusler structure for LaPdSb with the lattice constant theoretically estimated in Ref. [3]. Two isostructural and isoelectronic borderline compounds, $\text{La}(\text{Pt}_{0.5}\text{Pd}_{0.5})\text{Bi}$ and $\text{LaPt}(\text{Bi}_{0.2}\text{Sb}_{0.8})$, generate the continuous set of $\text{La}(\text{Pt}_{1-x}\text{Pd}_x)(\text{Bi}_{1-y}\text{Sb}_y)$ alloys which could be expected to appear at the topological borderline, if their compositions satisfy $y \approx 0.8 - 1.6 \cdot x$, marked by the straight red line in Fig. 1 a. To ensure this, we pick up the composition from the middle of the red line, i.e. $\text{La}(\text{Pt}_{0.75}\text{Pd}_{0.25})(\text{Bi}_{0.6}\text{Sb}_{0.4})$, which exhibits the close proximity to the phase transition as indicated by its calculated BSF in Fig. 1 d. In principle, it is possible to establish one more path from LaPtBi into the trivial phase, by manipulating the early transition element, i.e. by substituting La with e.g. Sc. Thus, generally, the manifold of possible borderline compositions will represent a two-dimensional surface in a three-dimensional parameter space.

By comparing all three BSFs presented in Fig. 1, one finds several similar features. One of them is the presence of a Dirac cone centered almost at the Fermi energy (E_F) in the Γ point of the Brillouin zone, which indicates their topological phase transition state. Since all compounds show a considerable amount of chemical disorder, one observes noticeable broadening of the spectral intensity, especially within the energy regime where the spectral intensity is strong, i.e. approximately from 0.25 eV above and from -0.8 eV below E_F . By approaching E_F the broadening reduces leaving the conical bands to remain Bloch-like. Another interesting feature are the dispersionless impurity-like states, recognized as horizontal stripes which become more distinct within the regime closer to E_F . They remind the resonant impurity levels observed in the gapless semiconductors as e.g., in PbTe host doped by Tl or Ti, and play an important role in tuning of thermoelectric properties [18]. On a first glance, the cases considered here may seem to be different, since the chemical disorder rates are very high, thus in the context of the chemical composition the impurities are formally absent. One can however straightforwardly see that the impurity-like effects occur at arbitrary disorder rate, since any chemically-disordered system can be approximated by the translational-invariant regular system to any limit. This can be achieved, for instance, by subsequent accumulation of different chemical configurations within the correspondingly expanded translational supercell. Once the difference between the disordered original and the translational-invariant systems which actually contains randomness (the so-called self-energy, if the “difference” is treated in terms of the Green functions) appears to be small enough, it must produce nothing else but the effect of random impurities embedded in the “host” represented by the translational-invariant system.

The BSFs presented in Figure 1 reveal, that by moving away from E_F the density of resonant levels increases; in the energy regime where the DOS becomes sufficiently large, they approach each other close enough to merge

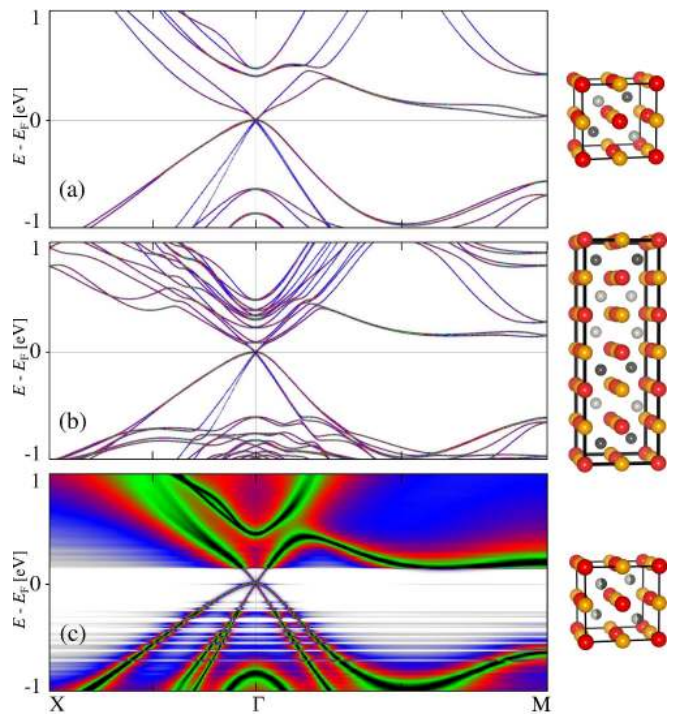


FIG. 2: Comparison of the electronic structures of the same $\text{La}(\text{Pt}_{0.5}\text{Pd}_{0.5})\text{Bi}$ composition, but related to the different chemical orders. Corresponding crystal structure units are shown on the left. Red and yellow spheres mark La and Bi atoms, gray and dark-gray - Pd and Pt, respectively. (a) The smallest possible ordered structure (8 nonequivalent atoms within unit cell) of the given stoichiometry, in which half of the tetrahedral sites are occupied by Pt, half - by Pd. (b) More complicated ordered variant of the same composition with 24 nonequivalent atoms which includes more environmental combinations. (c) The system with fully random Pd/Pt disorder (random occupation of the tetrahedral sites by Pt/Pd is indicated by the half-dark/half-light-gray spheres, respectively).

into a continuum. This situation is typical for the conventional metallic alloys, where the distinct resonant levels cannot be easily observed. In contrast to conventional metals, here in the vicinity of E_F the DOS is strongly reduced, and the impurity levels become evident. At the same time, they remain resonant (i.e., not isolated) since the semimetals do not exhibit the energy gap.

Based on the same arguments as we have used above, we can decompose our original disordered system (represented by CPA in Fig. 1 b or in Fig. 2 c) into a translational-invariant “host”, which is close enough in the sense of the same borderline behavior, plus the remaining self-energy representing randomness. In case of the disordered $\text{La}(\text{Pt}_{0.5}\text{Pd}_{0.5})\text{Bi}$ alloy, such a “host” can be already represented by the minimal ordered system shown in Fig. 2 a. We can continue this procedure by including more random combinations (Fig. 2 b) in the unit cell by approaching the electronic structure to the original situation in Fig. 2 c. The randomness, which in this

case becomes relatively small, will have a strong broadening effect only within those energy regimes where the large spectral weight of the host states is contained (at those energy levels, where many distinct eigenstates are situated closely to one another), i.e. far away from E_F , and thus, far from the conical bands. In this context, it becomes clear why these conical bands are so “insensitive” to disorder in terms of CPA. The reason is that their presence is an intrinsic property of the ordered “host” system and the randomness, which strongly affects only the energy range with a large DOS, cannot destroy it. At most, what may occur in the low DOS region, are rather weak disorder effects, as e.g., the appearance of the distinct impurity levels. In particular, one impurity level will be formed in the Γ point at E_F , due to the four-fold degeneracy of the corresponding eigenstates.

By inspecting the BSF in the meV regime (Figs. 3 a, b) the structure of the impurity level in the vicinity of E_F appears to be rather complicated: it consists of three distinct peaks produced mostly by mixture of the $p_{3/2}$ - and the d -states as well as of the relatively broad set of smaller peaks of the s -states spread almost equally over all atomic types. It indicates that the impurity levels stem not just from particular atoms, but rather from hybridized orbitals which include contributions from all types of atoms constituting the formula unit, as it occurs in the zinc-blende, rock-salt and thus in the Heusler structures.

We notice, that all above considerations are restricted only to those types of disorder, which affect the translational symmetry, but not the chemistry of a compound or the topology of a lattice (so, that a system can still be considered as an 18 electron half-Heusler).

On the next step we will study the transport characteristics, which appear to be unusual due to a rich combination of different electronic structure features in the vicinity of E_F .

V. TRANSPORT CHARACTERISTICS

Here we will study the electron transport characteristics of $\text{La}(\text{Pt}_{0.5}\text{Pd}_{0.5})\text{Bi}$ by calculating the residual conductivity by means of the general Kubo formalism [19, 20]:

$$\begin{aligned} \sigma_{\mu\nu} = & \frac{\hbar}{\pi V} \text{Tr} \left\langle \hat{J}_\mu \Im G^+ \hat{j}_\nu \Im G^+ \right\rangle \\ & + \frac{i\hbar}{2\pi V} \text{Tr} \left\langle \left[\hat{J}_\mu \Im G^+ \hat{j}_\nu - \hat{J}_\nu \Im G^+ \hat{j}_\mu \right] \Re G^+ \right\rangle \\ & + \frac{e}{2\pi V} \text{Tr} \left\langle \Im G^+ \left(r_\mu \hat{J}_\nu - r_\nu \hat{J}_\mu \right) \right\rangle, \end{aligned} \quad (1)$$

where $\Re G^+$ and $\Im G^+$ are the Hermitian and anti-Hermitian components of the retarded Green function G^+ ; \hat{J}_μ and \hat{j}_μ are the spatial μ -components of the general response, i.e. spin- and charge-currents, respectively. The brackets $\langle \rangle$ mean the configurational average required in case of random disorder. The first term (so-

called Kubo-Greenwood term) is symmetric and thus is responsible for the longitudinal conductivity (expressed by the diagonal part of the conductivity tensor). The second and the third terms are antisymmetric and thus contribute to the off-diagonal conductivities. Since the first and the second terms contain the configurational average over the products of Green functions, in case of disorder they normally need systematic improvement (the so-called vertex corrections, which we take into account). This is, however is not necessary for the last term - its configurational average reduces to the average of single Green function as delivered by CPA. Assuming the zero-temperature case, the longitudinal conductivity is precisely given by the first term evaluated at E_F . In case of the zero DOS at E_F (i.e., in the semiconductor case) it is precisely zero. The same holds for the second (antisymmetric) term. The third term in general is non-zero, even in case of the zero-temperature semiconductor, as it contains contributions from the occupied states (so-called “Fermi-sea” contribution). It was demonstrated by Středa [21] that it is possible to include the Fermi-sea contributions by using the Green function at E_F due to its analytical properties. The Středa formulation is exact only for the conserving currents (the transverse charge currents, such as e.g. the Fermi-sea contributions to the ordinary or anomalous Hall effects). For the spin current, which in general is a non-conserving quantity in the bulk, it is only an approximation which assumes that the non-conserving component of the spin current vanishes.

In order to access the spin-resolved off-diagonal components $\sigma_{xy}^{\uparrow(\downarrow)}$, where the spin polarization \uparrow (\downarrow) refers to the z -axis, we employed the relativistic scheme [20, 22]. Due to the small DOS in the vicinity of E_F the numerical error in E_F position may be relatively large, for this reason it makes sense to perform the calculations of the longitudinal $\sigma = \sigma_{xx} = \sigma_{yy}$ and the spin Hall $\sigma_{\text{SH}} = \sigma_{xy}^{\uparrow} - \sigma_{xy}^{\downarrow}$ conductivities as functions of energy within a finite energy window centered at E_F . The results for σ , σ_{SH} , and the spin Hall angle, $\sigma_{\text{SH}}/\sigma$, are shown in Figs. 3 c, d and e, respectively. Since the disorder-induced broadening in this energy window is also small, we will compute our transport quantities by adding a small imaginary constant $\delta = \text{Im}E$ to the energy E , and then subsequently decreasing it. Smaller δ value will result into a stronger oscillation of all energy-dependent quantities and the converged calculation will require more k -points. For example, in case of $\delta = 1$ meV, the k -mesh density was increased up to 10^6 , and in case of $\delta = 0.1$ meV – to 10^7 points in the irreducible wedge of the Brillouin zone. By setting the δ value completely to zero, the remaining broadening would be plainly disorder-induced, however at $E \approx E_F$ this effect becomes so small, that the well-converged calculation of residual conductivities would require an enormous number of k -points. For this reason we limit our analysis to the results for $\delta = 1$ and 0.1 meV.

As follows from Fig. 3 c, the mean amplitudes of σ and σ_{SH} as functions of energy within $E < E_F$ strikingly de-

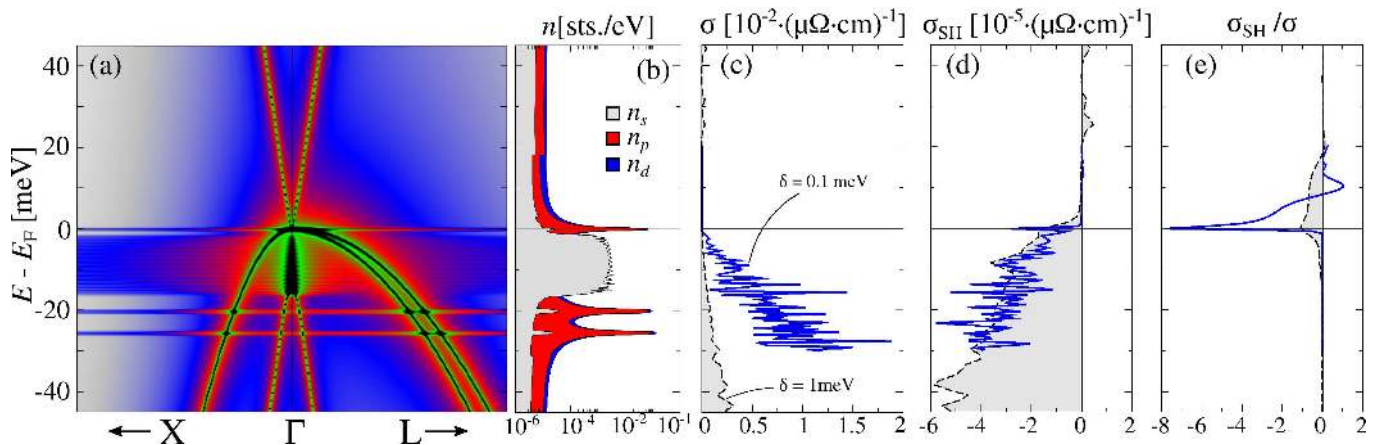


FIG. 3: (a) Calculated BSF for La(Pt_{0.5}Pd_{0.5})Bi alloy (spectral intensity distribution is the same as in Fig. 1) and (b) the corresponding s -, p - and d -projected DOS shown using the logarithmic scale ($n_{s,p,d}$ - in gray, red and blue, respectively). (c) Diagonal conductivity σ , spin Hall conductivity σ_{SH} , and their ratio σ_{SH}/σ (spin Hall angle), calculated as functions of the energy E . Black dashed line corresponds to the small imaginary energy offset $\delta = 1$ meV, thick blue line - to $\delta = 0.1$ meV.

crease by approaching E_F . To a large extent this results from the DOS of the parabolic-shaped dispersion of the hole-like states. As follows from the BSF in Fig. 3 a, they are Bloch-like and are perturbed by disorder only slightly, thus remaining highly conductive and making the most substantial contribution to σ , as well as to σ_{SH} (they consist mostly of p - and d -symmetries, and thus “feel” the spin-orbit coupling) despite their small DOS. By decreasing δ from 1 meV to 0.1 meV, the mean amplitude of σ is amplified by a factor of about 10 times (since these Bloch-like states become even more Bloch-like), however its decrease towards E_F becomes more steep by leading to the same small values at $E \approx E_F$. A more detailed plot in Fig. 4 a reveals that for $E \approx E_F$ this decrease is so steep that it produces even smaller σ values for $\delta = 0.1$ meV, thus the effects of δ -broadening within $E \geq E_F$ and $E < E_F$ are opposite to each other. Indeed, for $E \geq E_F$ the hole-like Bloch states are absent and σ is mostly defined by amplitudes of Lorentzian tails from the hole-like states penetrating into this energy regime due to finite δ (and disorder).

Another strong impact on transport characteristics is produced by the non-dispersive impurity-like states. Since they are localized, they almost do not contribute to σ , but significantly contribute to σ_{SH} . This is especially evident for $E = E_F$, where the hole-like Bloch-like states are absent. By decreasing δ , the Lorentzian tails get suppressed together with their contributions to σ and σ_{SH} , whereas the localized impurity states get unscreened and their contributions become, respectively, more pronounced. This is clearly manifested by the sharp peak of σ_{SH} at $E \approx E_F$ for $\delta = 0.1$ meV (Fig. 4 b).

Combination of these effects has interesting consequences for the spin Hall angle, σ_{SH}/σ , which exhibits a divergent behavior at $E \approx E_F$ (see Fig. 3 e) since $\sigma \sim \delta + \sigma^{imp}$, $\sigma_{SH} \rightarrow \sigma_{SH}^{imp}$ and $\sigma^{imp} \ll \sigma_{SH}^{imp}$, where “imp” refers to the impurity. For $\delta = 0$ the spin

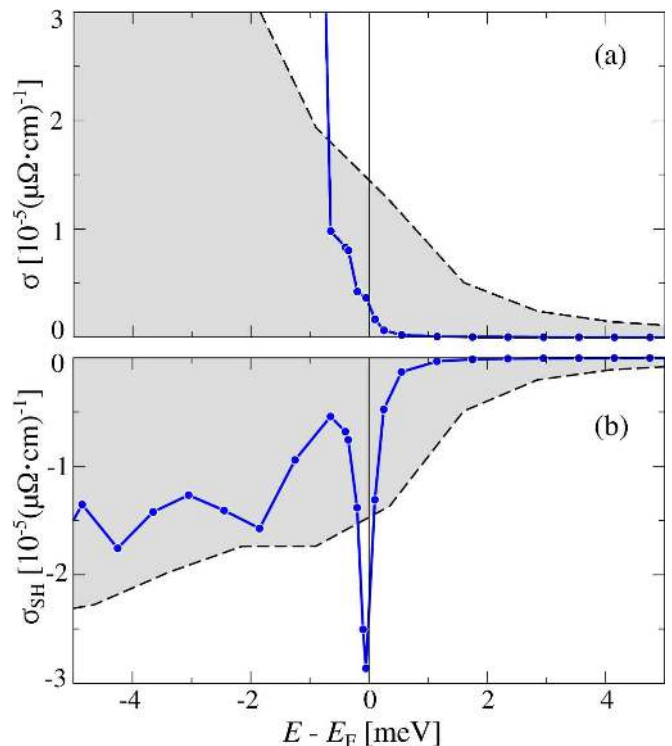


FIG. 4: (a) Longitudinal conductivity σ and (b) spin Hall conductivity σ_{SH} , calculated as functions of energy E . Black dashed line corresponds to the imaginary energy offset $\delta = 1$ meV, thick blue line - to $\delta = 0.1$ meV.

Hall angle will be maximized being limited only by small Lorentzian broadening coming from disorder. For $E < E_F$ the spin Hall angles are very small, even in the presence of impurities (seen at about -20 and -25 meV, see Figs. 3 a, b), since this situation is closer to that of a conventional metal, where σ is large due to Bloch-like

dominating contributions. For instance, as it was shown experimentally for Pt, it has quite large intrinsic spin Hall conductivity $\sigma_{\text{SH}} \sim 3 \cdot 10^{-4} (\mu\Omega \cdot \text{cm})^{-1}$, but also large $\sigma \sim 4 \cdot 10^{-2} (\mu\Omega \cdot \text{cm})^{-1}$ (bounded by remaining impurities and finite temperature effects), which leads to the spin Hall angle of about $\sim 10^{-2}$ [23]. Another set of the impurity states, seen as the sequence of many similar stripes confined within a range of about 15 meV right below E_{F} , does not contribute to σ_{SH} due to their s -symmetry.

The contribution of the conical states is difficult to distinguish: in the regime $E > E_{\text{F}}$, where only conical states exist, σ strongly scales down with δ , by indicating that σ is dominated by Lorentzian tails stemming from the parabolic states. On the other hand, by using the analogy with a charged particle moving in a magnetic field (which includes the effect of the spin-orbit coupling), the relaxation time approximation $\sigma_{xx} \sim \frac{ne^2}{\tau m} (\omega^2 - \frac{1}{\tau^2})^{-1}$, $\omega \sim B_{\text{so}}/m$, m - is the effective electron mass, shows that $\sigma \rightarrow 0$ for $m \rightarrow 0$, i.e., for massless particles. At the same time, the off-diagonal components $\sigma_{xy} \sim \frac{ne^2\omega}{m} (\omega^2 - \frac{1}{\tau^2})^{-1} \rightarrow \text{const}$, which does not depend on the scattering time τ , i.e. the massless electrons will propagate along the equipotential lines with constant velocity which depends on the spin-orbit coupling but does not depend on the disorder scattering rate. However even this possible contribution appears to be rather small, compared to the others. Indeed, despite that the conical bands look very much Bloch-like, it is very difficult to distinguish even their DOS. It is not only smaller than the DOS of the impurities, but it is also smaller than the DOS of the parabolic states for $E < E_{\text{F}}$, since in the vicinity of the E_{F} : $n_{\text{par}} \sim \sqrt{E - E_{\text{F}}} > n_{\text{conical}} \sim (E - E_{\text{F}})^2$.

VI. SUMMARY AND OUTLOOK

Our detailed electronic structure calculations for the $\text{LaPt}_{0.5}\text{Pd}_{0.5}\text{Bi}$ alloy suggest that the topological borderline half-Heusler bulk systems with chemical disorder will necessarily exhibit impurity-like resonant states, with one of them located at the top of the valence band, which will coincide with the Dirac point at E_{F} due to statistical restoring of the cubic symmetry. Such electronic structure leads to a strong sensitivity of the electronic transport characteristics with respect to the position of E_{F} , which might easily fluctuate in experiments. According to the presented first-principles calculations based on the Kubo formalism, once the Fermi energy sticks to the impurity level, it will result in a strong suppression of the longitudinal conductivity σ , but will retain the off-diagonal spin Hall components σ_{SH} , thus leading to divergent spin Hall angles $\sigma_{\text{SH}}/\sigma$. As we have seen, the suppression of σ strongly depends on the amplitude of the Lorentzian tails from the parabolic Bloch-like states below the Fermi energy, which efficiently screen the impurity effect. For this reason, the divergent behavior

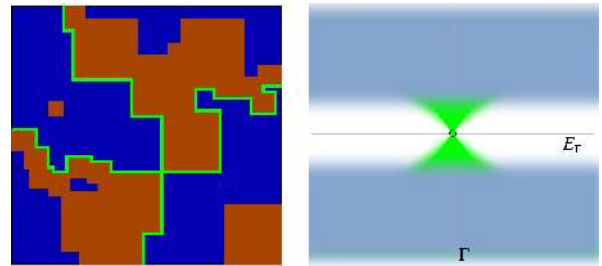


FIG. 5: The sketch of a topologically phase-separated disordered system (in two dimensions) at the percolation transition. Dark-blue and brown clusters represent topologically distinct phases. The system contains two distinct “infinite” clusters (connecting the opposite sites of a square situated infinitely far from each other). The green line marks the infinite topological transition interface path along which the inversion of the energy levels occurs. The BSF of such system (corresponding already to a three-dimensional case, sketched on the right) will impose the Dirac state centered at E_{F} (colored as green, the rest of the electronic states corresponds to the gray area); the broadening of the spectral density reduces by approaching the Dirac point.

of the spin Hall angle seems to be an essentially low-temperature feature when the additional broadening of the Bloch-like states due to phonons is sufficiently weak. The conical-dispersive Dirac bands appear to remain Bloch-like in agreement with arguments in Refs. [11, 12] and do not exhibit any impurity-like effects, except the regime $E \leq E_{\text{F}}$ where they are perturbed by the impurities connected with the parabolic bands. At the same time, despite of their proximity to the Bloch states, their own contribution to the conductivity components appear to be negligibly small compared to the effects from the Lorentzian tails and the resonant impurities. We stress, that the topological properties play here an important, though an auxiliary role. In the nontrivial phase the system would exhibit the impurity level at E_{F} as well, however due to the proximity of the parabolic like bands (not only hole-like, but also electron-like ones) the Lorentzian screening of the impurity will be too strong. On the other hand, in the trivial case, E_{F} would be placed in the band gap, i.e. above the impurity level.

So far we have considered the properties of the homogeneously disordered bulk systems, in which the bulk Dirac state is unstable with respect to the stoichiometric variations. On the other hand, modeling of the inhomogeneous disordered borderline systems may help to overcome this problem. Let us consider the sketch in Fig. 5, where the disordered system is interpreted as a topologically phase-separated system consisting of random clusters with trivial and nontrivial order of their eigenstates. The topological inversion of states will inevitably occur at the interface between topologically distinct clusters, which represents a randomly curved two-dimensional manifold. Since the Dirac points distributed on this surface will possess a two-dimensional nature, all considerations related to their topological protection

and the corresponding transport properties of the typical Dirac surface states can be expected. The whole material will belong to the borderline topological state only, if it contains at least two infinite connectible topologically distinct clusters, since this guarantees an infinite and isotropic spread of the Dirac-point surface, i.e. that it always connects the opposite sides of a sample. The statistical conditions guaranteeing the existence of such clusters are provided by percolation theory [24]. For example, in case of two-dimensional systems, the borderline state cannot be stabilized with respect to the composition since it requires the relative amounts of both phases to be precisely equal. For example, with respect to $\text{La}(\text{Pt}_{1-x}\text{Pd}_x)\text{Bi}$ alloys, the compositions with $x \neq 0.5$

will correspond to either trivial or topological behavior of the whole system. In case of the three-dimensional systems, the percolation will persist within a large compositional range, $0.17 < x < 0.83$, which greatly softens the restrictions for their experimental synthesis.

Acknowledgments

The work was financially supported by the Deutsche Forschungsgemeinschaft Schwerpunktprogramm DFG-SPP 1666.

-
- [1] S. Chadov, X.-L. Qi, J. Kübler, G. H. Fecher, C. Felser, and S.-C. Zhang, *Nature Materials* **9**, 541 (2010).
 - [2] H. Lin, L. A. Wray, Y. Xia, S. Xu, S. Jia, R. J. Cava, A. Bansil, and M. Z. Hasan, *Nature Materials* **9**, 546 (2010).
 - [3] W. Al-Sawai, H. Lin, R. S. Markiewicz, L. A. Wray, Y. Xia, S.-Y. Xu, M. Z. Hasan, and A. Bansil, *Phys. Rev. B* **82**, 125208 (2010).
 - [4] C. Tunkay and M. Tomak, *Solid State Commun.* **50**, 1065 (1984).
 - [5] I. M. Tsidilkovski, G. I. Harus, and N. G. Shelushinina, *Adv. Phys.* **34**, 43 (1985).
 - [6] M. Orlita, D. M. Basko, M. S. Zholudev, F. Teppe, W. Knap, V. I. Gavrilenko, N. N. Mikhailov, S. A. Dvoretzkii, P. Neugebauer, C. Faugeras, et al., *Nat. Physics* **10**, 233 (2014).
 - [7] M. G. Haase, T. Schmidt, C. G. Richter, H. Block, and W. Jeitschko, *J. Solid State Chem.* **168**, 18 (2002).
 - [8] T. Oguchi, *Phys. Rev. B* **63**, 125115 (2001).
 - [9] T. Sekimoto, K. Kurosaki, H. Muta, and S. Yamanaka, *Mat. Transactions* **48**, 2079 (2007).
 - [10] S. Chadov, J. Kiss, J. Kübler, and C. Felser, *Phys. Stat. Sol. RRL* **7**, 1 (2012).
 - [11] A. Narayan, D. D. Sante, and S. Picozzi, *Phys. Rev. Lett.* **113**, 256403 (2014).
 - [12] D. Di Sante, P. Barone, E. Plekhanov, S. Ciuchi, and S. Picozzi, *Sci. Reports* **5**, 11285 (2015).
 - [13] H. Ebert, D. Ködderitzsch, and J. Minár, *Rep. Prog. Phys.* **74**, 096501 (2011).
 - [14] P. Soven, *Phys. Rev.* **156**, 809 (1967).
 - [15] D. W. Taylor, *Phys. Rev.* **156**, 1017 (1967).
 - [16] J. P. Perdew, K. Burke, and M. Ernzerhof, *Phys. Rev. Lett.* **77**, 3865 (1996).
 - [17] W. Wong-Ng and J. Yang, *Powder Diffraction* **28**, 32 (2012).
 - [18] J. P. Heremans, B. Wiendlocha, and A. M. Chamoire, *Energy Environ. Sci.* **5**, 5510 (2012).
 - [19] W. H. Butler, *Phys. Rev. B* **31**, 3260 (1985).
 - [20] S. Lowitzer, M. Gradhand, D. Ködderitzsch, D. V. Fedorov, I. Mertig, and H. Ebert, *Phys. Rev. Lett.* **106**, 056601 (2011).
 - [21] P. Středa, *J. Phys. C: Solid State Phys.* **15**, L717 (1982).
 - [22] A. Vernes, B. L. Györfy, and P. Weinberger, *Phys. Rev. B* **76**, 012408 (2007).
 - [23] M. Isasa, E. Villamor, L. E. Hueso, M. Gradhand, and F. Casanova, *Phys. Rev. B* **91**, 024402 (2015).
 - [24] S. Kirkpatrick, *Rev. Mod. Phys.* **45**, 574 (1973).